Available online at www.sciencedirect.com

ScienceDirect

Transportation Research Procedia 55 (2021) 1114–1121

Transportation Research Procedia

www.elsevier.com/locate/procedia

14th International scientific conference on sustainable, modern and safe transport

Experimental and Numerical simulation of a Three Point Bending Test of a Stainless Steel Beam

Daniel Jindra[a]*, Zdeněk Kala[a], Jiří Kala[a], Stanislav Seitl[b]

[a]*Institute of Structural Mechanics, Brno University of Technology, Veveří 331/95; 602 00, Brno; Czech Republic*
[b]*Institute of Physics of materials, Czech Academy of Sciences, Žižkova 22; 616 62, Brno, Czech Republic*

Abstract

An advanced simulation process of a stainless steel member in ANSYS technology is described in this paper. A three-point bending test of a hot rolled stainless steel material grade 1.4301 (AISI 304) member has been conducted. The cross-section of the beam was IPE80, with the span of the supports equal to 240 mm. The results of the experimental test were compared with the materially and geometrically nonlinear numerical analysis. In order to describe the behavior of the stainless steel material, the Ramberg and Osgood model has been adopted along with multi linear stress-strain description with isotropic hardening feature. The finite element model has been created using software ANSYS classic APDL environment, and the results were compared.

Keywords: Stainless steel; Three-point bending test; Finite element analysis; Ramberg and Osgood model

1. Introduction

Due to its resistance against corrosion, the stainless steel as a material has a high potential in various civil engineering applications, also many transport structures, e.g. bridges, footbridges, as closely discussed by Baddoo (2008). According to a recent cost-efficiency study conducted by Daghas et al. (2019), the usage of certain stainless steel is the most beneficial in cases of bridges exposed to aggressive environmental conditions with heavy traffic volumes. The aim of the article is to describe a robust design procedure with the appropriate use of numerical and experimental simulation.

* Corresponding author. Tel.: +420 54114 7382 (the office of prof. Ing. Zdeněk Kala Ph.D.)
E-mail address: jindra.d@fce.vutbr.cz

10.1016/j.trpro.2021.07.183

The test data of stainless steel are less numerous in comparison with an ordinary carbon steel. Also, unlike standard steels, the stainless steel as a material has no sharp yield point and its material behavior is rather described by much rounded stress-strain curve, with much higher ductility than in cases of the most common standard carbon steels. As the equivalent of the yield stress, 0.2% proof stress is adopted in a conventional steel design. However, conventionally widely adopted description of the stress-strain behavior by a bilinear material model does not recognize the significant material hardening alongside with fulfilling the sufficient reliance in the design.

Due to its high costs compared to ordinary carbon steel, much detailed material behavior description needs to be adopted in order to design more cost-efficient stainless steel structures. Therefore, a closer investigation of structural performance of stainless steel members exposed to various types of loading is a suitable area of the research. Experimental tests of stainless steel hollow sections have been documented in a study by Gardner (2004). Numerical finite element analyses of cold-formed stainless steel CHS columns of various cross-sections in compression with determination of revised buckling curves and comparison with comprehensive experimental program results have been performed and well documented by Buchanan et al. (2018). Eccentricities in the compressive loading of these CHS columns have been incorporated in the subsequent study by Buchanan et al. (2020). Recently, a wide statistical study of not only material characteristic values has been conducted by Arrayago et al. (2020).

In this study, the three-point test of a simply supported stainless steel beam is analyzed numerically, and the results are compared with the experimental data. Material of the specimen is hot rolled stainless steel grade EN 1.4301 (AISI 304), the cross section of the beam is IPE80, and the span of the supports is 240 mm.

2. Experimental tests in three-point bending

Material properties and chemical composition of the stainless steel specimens (grade EN 1.4301 / AISI 304) based on the inspection certificate (attest of Montanstahl AG, certificate no. 127381-00, in accordance with EN 10204 3.1, size standard EN 10034, product standard EN 10365) are summarized in the table 1 below.

Table 1. Chemical composition and material properties of the stainless steel specimens.

Specimen	C	Si	Mn	P	S	Ni	Cr	N	Tensile strength (MPa)	0.2% proof stress (MPa)	1.0% proof stress (MPa)	Elongation (%)
Specimen 1	0.030	0.36	1.51	0.030	0.002	8.00	18.30	0.060	675	342	380	55
Specimen 2	0.017	0.44	1.55	0.027	0.002	8.00	18.20	0.050	628	255	319	58

Experimental test in three-point bending have been conducted using 2 specimens of the IPE80 cross-sectional simply supported beam with the span distance of 240 mm. The loading has been applied in the mid-span of the beam, conducted by a displacement increasing with constant speed of 0.5 mm/min. So far only little number of the test specimens has been documented in order to provide a proper statistical evaluation. The experimental set-up and monitored results (force-displacement relation) are depicted in the Fig.1 below. Vertical displacement has been monitored in the bottom surface mid-span of the beam member. Both specimens are the same material (EN 1.4301), however from different batches, therefore slightly different material properties (Table 1). In both examined cases, also the local bending of the beam web along the beam longitudinal axis has occurred (see also Fig.7 b). This local stability loss has developed shortly after reaching the ultimate load in case of the specimen 1. However, in case of the specimen 2, this feature has developed along with the initiation of the plastic behavior, approximately under the loading force of 50 kN (Fig.1 a). Therefore, further force-displacement data points of the specimen 2 response are absent. It is not excluded, there were a certain initial imperfections of the specimen 2 beam web.

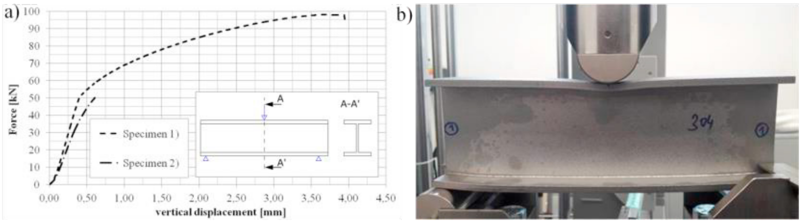

Fig. 1. (a) measured force mid-span displacement dependence; (b) experimental set up.

3. Numerical FE model

In order to conduct geometrically and materially nonlinear numerical analyses, a parametrical finite element model has been created using software ANSYS, in the environment of Classic APDL (Ansys, 2018).

3.1. Geometry of the FE model

To model the IPE80 beam, 4-nodal structural shell elements (SHELL 181) with total of 6 degrees of freedom (3 translational and 3 rotational) per each node have been used. These elements possess bending and membrane stiffness (MIndlin-Reissner theory). Reduced integration with 1 integration point (3 through the thickness) and hourglass control have been considered. The geometrical shapes of all the finite elements were rectangles, with maximal edge size of 10 mm in the longitudinal direction (along the beam axis), and maximal edge size of 8 mm in both of the cross-sectional directions (also see Fig.4).

No initial geometrical imperfections, neither global nor local have been incorporated into the FE model yet.

3.2. Material model

Suitable description of the stress-strain behavior of the stainless steel material is in accordance with the relation proposed by Ramberg and Osgood (1943), later modified by Hill (1944):

$$\varepsilon = \frac{\sigma}{E_0} + 0.002\left(\frac{\sigma}{\sigma_{0.2}}\right)^n , \tag{1}$$

where σ and ε are the engineering stress and strain respectively, E_0 is the elastic Young's modulus, $\sigma_{0.2}$ is the material 0.2% proof stress (the equivalent of the yield strength), and n states for a strain hardening exponent. Material behavior in accordance with this formulation results in a nice agreement with the experimental data of the stainless steel specimens for stress values up to $\sigma_{0.2}$ value. However, according to the results of various studies, e.g. the one by Gardner (2001), at higher strains, the model overestimates the stress values. A compound two stage stress-strain curve devised by Mirambell and Real (2000) provides better agreement with the stress-strain experimental data for stress values above the 0.2% proof stress value in accordance with various studies, e.g. the one by Garden (2001). The second stage of this relation is defined as:

$$\varepsilon = \frac{\sigma - \sigma_{0.2}}{E_{0.2}} + \left(\varepsilon_{tu} - \frac{\sigma_u - \sigma_{0.2}}{E_{0.2}} - \varepsilon_{t0.2}\right)\left(\frac{\sigma - \sigma_{0.2}}{\sigma_u - \sigma_{0.2}}\right)^{n'0.2,u} + \varepsilon_{t0.2} \Leftrightarrow \sigma > \sigma_{0.2} , \tag{2}$$

where σ_u is the ultimate strength of the stainless steel, $n^{'0.2,u}$ is a strain hardening exponent, $\varepsilon_{t0.2}$ is the total strain at the 0.2% proof stress, ε_{tu} is the total strain at ultimate stress, and $E_{0.2}$ is the stiffness (tangent modulus) at the 0.2 % proof stress given as:

$$E_{0.2} = \frac{E_0}{1 + 0.002 \cdot n \cdot E_0 / \sigma_{0.2}} . \tag{3}$$

The description of the material behavior in accordance with the equations 1 and 2 is well applicable in tension, however, in case of both types of the loading, tension and compression, a certain modification of the Eq. 2 is proposed, as recommended in a study by Gardner (2004). Instead of the σ_u value, the 1% proof stress $\sigma_{1.0}$ is used, alongside with an appropriate strain hardening exponent $n^{'0.2,1.0}$, and the relation is in the shape of:

$$\varepsilon = \frac{\sigma - \sigma_{0.2}}{E_{0.2}} + \left(0.008 - \frac{\sigma_{1.0} - \sigma_{0.2}}{E_{0.2}}\right)\left(\frac{\sigma - \sigma_{0.2}}{\sigma_{1.0} - \sigma_{0.2}}\right)^{n'0.2,1.0} + \varepsilon_{t0.2} \Leftrightarrow \sigma > \sigma_{0.2} . \tag{4}$$

A multi-linear material model with isotropic hardening (Von Mises plasticity) has been considered for the purpose of the numerical analyses. Closer description of this material model implementation via APDL parametric macro is described in author's previous study (Jindra, 2020). However, in order to neglect the plasticity at low strain values (from an engineer's point of view), in this study, the stress-strain behavior only up to value of 0.5 $\sigma_{0.2}$ has been considered as ideal elastic instead of up to 2/3 $\sigma_{0.2}$ value, which has been adopted previously (Jindra 2020), and in some cases of material parameter values and geometries has not led to such a favorable results.

The engineering (nominal) stress-strain material curves are required to be transferred into true stress and logarithmic strain dependencies in order to be in a match with the results of geometrically nonlinear FE analyses:

$$\sigma_{true} = \sigma_{nom}(1 + \varepsilon_{nom}) , \tag{5}$$

$$\varepsilon_{true} = ln(1 + \varepsilon_{nom}) , \tag{6}$$

where σ_{nom} is the engineering (nominal) stress, ε_{nom} is the nominal engineering strain. σ_{true} and ε_{true} are true stress and true total (mechanical) strain respectively. Negative values of ε_{nom} need to be input in order to define the compressive material properties.

Figure 2 depicts the two approaches of the adaptation of the multi-linear material model, approach #A and #B. In case of the approach #A, the stress-strain relation is defined in accordance with Eq. 1 and Eq.2. Approach #B considers the Eq. 1 and Eq. 4 instead. For both approaches, the stress-strain relation is depicted in accordance with given equations analytically (colorful graphical curves). Also, for both approaches, the blue curve represents the engineering stress-strain relation, the red curve represents the true stress-strain relation for compressive loading, and the stress-strain relation for tensile loading is represented by the green curve (in accordance with Eq. 5 and 6). In order to verify the material model APDL macros used for the further analyses, one-element tensile and compressive tests have been conducted, and the numerical results are described by the dash-dotted black curves in the Fig.2.

Due to the fact, that it is impossible to define a negative tangent of stress-strain relation while adopting isotropic hardening (Ansys, 2018), the true stress-strain relation in case of the compressive loading has been defined as ideal plastic (with the tangent of the stress-strain curve very close to 0, but positive) instead of any kind of softening, after the peak stress has been reached. Two examples of such material model APDL macro verifications conducted on one element FE tests are depicted in the Fig.2 a) and b) (for both approaches #A and #B), by dash-dotted black curve (the analytically defined relations follow the red curves). From an engineer's point of view, the difference between these two stress-strain curves is very negligible for strain values which are realistically expected to occur in structural analyses. The difference between these curves is recognizably increasing for strains above 20%. Instead of this approach, it is also possible to use the kinematic hardening feature in order to define also the negative tangent of the stress-strain curve while defining the material compressive behavior in true stress-strain values, however, this approach seemed to have more convergence problems after the peak compressive stress had been reached, and therefore, it has not been incorporated by the author of this study in the research.

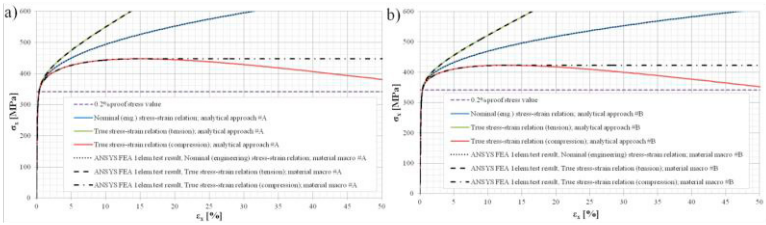

Fig. 2. Stress-strain relation verification: (a) for approach #A (Eq.1 + Eq.2); (b) for approach #B (Eq.1 + Eq.4).

The difference in stress-strain relations defined either in accordance with approach #A or approach #B is depicted in Fig.3 considering the engineering (nominal) stress-strain relation. In order to run these one-element verification tests, the following material parameter values have been adopted: $\sigma_{0.2}$ = 342 MPa; $\sigma_{1.0}$ = 380 MPa; σ_{u} = 675 MPa; ε_{tu} = 55%, based on the Table 1 of this document. Further parameters, as well as the Ramberg-Osgood parameters, have been based on the study by Arrayago (2020). The mean parameter values for austenitic stainless steels have been considered: E_0 = 195.416 GPa; n = 10.6; $n'^{0.2,u}$ = 2.3. However, in the study by Arrayago (2020), only parameters for a stress-stain description what is referred here as approach #A, have been discussed. Therefore, the parameter $n'^{0.2,1.0}$ required for approach #B has been considered by the same value as the parameter $n'^{0.2,u}$. Usually, these parameters have similar values in the majority of cases, e.g. parameter values in the study by Buchanan (2018), or previous material parameter identification study by Jindra (2020), and the differences in this parameter have more significant impact on the stress-strain curve shapes only for strain values approximately above 3%.

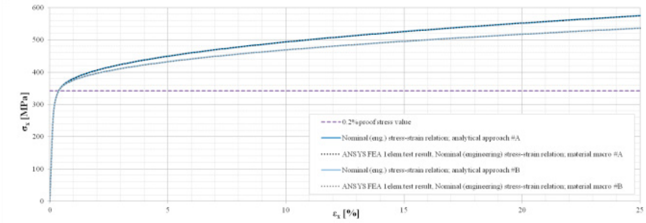

Fig. 3. Comparison of the nominal (engineering) stress-strain curves defined in accordance with approaches #A and #B.

One difficulty of the multi-linear material model with isotropic hardening which has been adopted in this study is the fact, that it is not possible to define different stress-strain relations for tensile and compressive loading. Certain alternative considering the adaptation of a different material model which enables this feature is available (Ansys 2018), however, the suitability for stainless steel has not yet been tested by the author of this study. Therefore, for both of approaches #A and #B, FE analyses using three different material macros have been conducted (total 6 FEA numbered i) - vi) in the table 2): either the stress-strain relation is defined in the true values for the compressive type of loading, or in true values for the tensional loading, or in the engineering (nominal) values. The results are compared and discussed and provide valuable data for further research as well as conventional steel design. In case of expected structural failure due to either pure tensional or pure compressive loading, it is feasibly available to adopt this presented approach. However, one of the aims of this study is to test this approach also for case of bending, or more precisely, certain kind of combination of bending and shear failure (short span of the tested beam).

3.3. Boundary conditions, loading and solver set up

The static span of the beam is 240 mm, however, small cantilevers (3 mm) have been modeled at both ends of otherwise simply supported beam (see Fig.4). Translational degrees of freedom in the vertical (z) direction are constrained along lines of the supports (at bottom flanges). Horizontal translational degrees of freedom (DoF) in the axial direction (x) are constrained along one of these support lines. Horizontal translational DoF of the both middle nodes of these lines (where the web is connected to the flange) are constrained in transversal direction (y).

In the first step of the geometrically nonlinear analyses, the gravitational acceleration (9.81 ms^{-2}) has been applied. Loading conducted by a prescribed vertical displacement (z direction) has been introduced in the subsequent loading steps of the analyses (3 steps: 3 mm, 3 mm and 2 mm). The displacement has been introduced through the upper mid-span nodes along the whole width of the beam upper flange (7 nodes).

Minimal number of the sub-steps within one step of displacement loading has been set up as 100, maximal 250, initial 250, and the number of the iterations within one sub-step as 140.

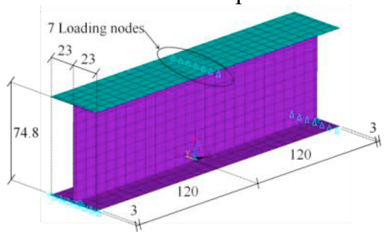

Fig. 4. Geometry of the FE model (in millimeters) and boundary conditions.

4. Results

Force-displacement dependence is depicted in the Fig.5. Loading force F is the summarization of all 7 forces from all 7 loading nodes (Fig.4). Vertical displacement has been monitored in the bottom surface mid-span node (where the origin of GSS is located in Fig.4). ultimate loads and corresponding displacements are summarized in the table 2. Plots from the last converged sub-step of case i) (as named in the table 2) are depicted in Fig.6 and Fig.7.

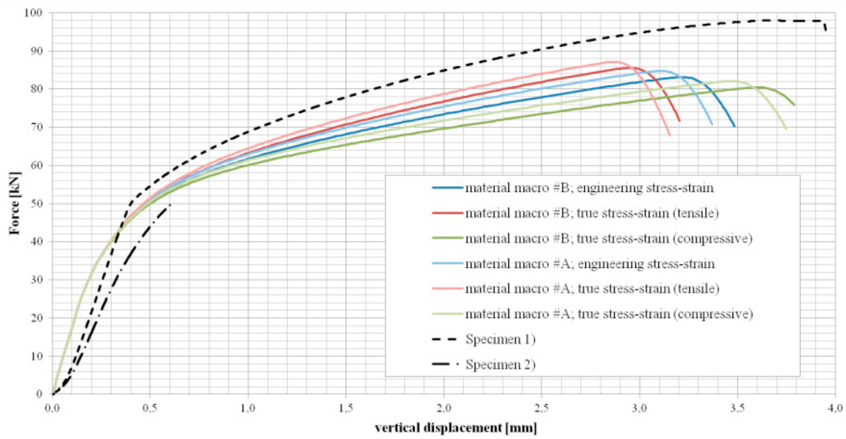

Fig. 5. Force-displacement dependence.

Table 2. Ultimate loads (forces F) and corresponding vertical displacements z.

Case	F_u (kN)	z_u (mm)
i) material macro #B; engineering stress-strain	83	3.2
ii) material macro #B; true stress-strain (tensile)	86	3.0
iii) material macro #B; true stress-strain (compressive)	80	3.6
iv) material macro #A; engineering stress-strain	85	3.1
v) material macro #A; true stress-strain (tensile)	87	2.9
vi) material macro #A; true stress-strain (compressive)	82	3.5
Specimen 1) (experimental values)	98	3.7

5. Discussion

In general, the results of the presented numerical finite element analyses (FEA) are in a good agreement with the experimental data (Fig.5, and Table 2). The value of the ultimate load determined by the FEAs was always smaller than the experimental value. However, there are not yet enough of experimental data to evaluate these results properly. Also the value of the corresponding mid-span bottom surface displacement was smaller in all the cases of FEAs. In the numerical analyses, the stiffness of the supports has not been considered, however this might have some influence during the experiment. The performance of both approaches #A and #B, which slightly differed in the stress-strain behavior definition for stress values above the proof stress (either in accordance with Eq.2 or Eq.4), is very similar for the adopted parameter values and the considered geometry of the structure. Ultimate forces F_u in the approaches #A are slightly closer to the experimental value, but the corresponding displacements z_u are slightly closer to the experimental value in cases of the approaches #B. It is not yet possible to determine which approach has a better performance, based only on one experimental result. More experiments need to be conducted in order to make such conclusion.

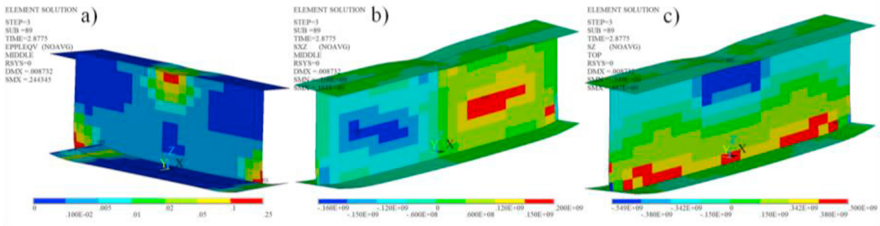

Fig. 6. FEA results: (a) Equivalent plastic strain (-); (b) Shear stress τ_{xz} (Pa); (c) Stress in vertical direction σ_z at the top element surface (Pa).

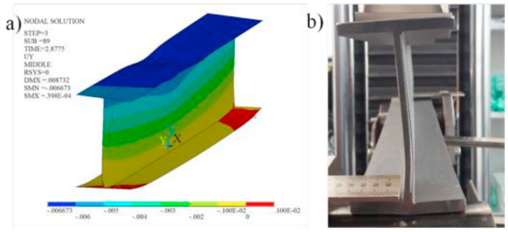

Fig. 7. (a) Horizontal displacements in transversal direction (along y axis); (b) IPE 80 beam after physical experiment.

In case of considered loading, the bending of a beam with significant shear stresses (Fig.6 b), there is noticeable difference in the results where different definitions of the stress-strain behavior (either true stress-strain for tensile loading, true stress-strain for compressive loading or engineering stress-strain relation) have been adopted. Even though the majority of equivalent plastic strains is below 0.5% (Fig.6 a), however, in some critical areas, the values are approximately 24%. As the failure is neither close to the pure tensional failure, nor to the pure compressive failure, in order to describe the material behavior more precisely while large strains are involved, it is necessary to use such material model, which enables a different behavior (stress-strain definition) in compression and tension. This will be performed in future research. However, for a conventional structural design of course, the adaptation of true stress-strain behavior for compressive loading always leads towards more conservative results.

In both, FEAs and experiment, the bending of the beam web along the beam longitudinal axis (x axis) has occurred. This is clearly visible in the Fig.7, where the transversal horizontal displacements (in y direction) are plotted (upper flange 6.7 mm shift). Also, as the reason of this bending, there are significant stresses in the vertical direction (global z direction) (Fig.6 c) in the top surfaces of the bottom web elements (max. 467 MPa). Note: top surfaces of these elements are those which the y axis of the global coordinate system is pointing towards (Fig.6 c).

6. Conclusion

A three-point bending test of IPE80 stainless steel specimen, material grade EN 1.4301 (AISI 304), has been conducted physically as well as numerically by FEAs in ANSYS. Two different approaches in definition of the stress-strain relations by adopting the Ramberg-Osgood and extended parameters have been considered. The results for these approaches (here stated as #A and #B) are negligible for the modeled case. Also, such a material model has been implemented which has no availability to define a different true stress-strain behavior for compression and tension. Instead, material macros considering the stress-strain behavior defined in order to describe either purely compressive or purely tensile loading (in the matter of true stress-strain values) or engineering (nominal) values have been implemented so far. The results concerning differences between these approaches are noticeable and discussed. In order to describe the material behavior more precisely also in combined type of loading (bending, shear, combination of tension and compression), a material model with availability to define a different tensile and a different compressive stress-strain behavior needs to be implemented. This will be part of the subsequent research. In case of conventional steel design, it is conservative approach to always adopt the true stress-strain relation determined for the compressive loading, and still the significant material hardening is captured, rather than adopting the much more simplified linear elastic ideal plastic stress strain curve (see the 0.2% proof stress value in Fig.2).

Overall, the numerical model responses are in a satisfying match with the experimental data (Fig.5, Fig.7, Table 2). The exact numerical description of the physical experiment is very difficult. The real behavior of the loading machine and boundary conditions (stiffness), would require rather detailed numerical analysis, with decreased utilization possibilities in conventional structural analyses. Rather larger number of the test specimens needs to be documented in order to provide a proper statistical evaluation, yet a limited number was so far available.

Acknowledgements

This paper has been created with the financial support of Czech Science Foundation by project No.: 20−00761S "Influence of material properties of stainless steels on reliability of bridge structures". Additional support was provided by the Brno Uni. of Tech. fund for specific university research, the project number FAST-J-21-7169.

References

Ansys, Inc. (2018) ANSYS 19.0. Canonsburg, PA 15317 U.S.A.

Arrayago, I., Rasmussen, K.J.R., Real, E., 2020. Statistical analysis of the material, geometrical and imperfection characteristics of structural stainless steels and members. Journal of Constructional Steel Research vol.175, ISSN: 0143-974X. doi:10.1016/j.jcsr.2020.106378.

Baddoo, N.R., (2008). Stainless steel in construction: A review of research, applications, challenges and opportunities. Journal of Constructional Steel Research vol. 64 iss.11 p.1199-1206. ISSN: 0143-974X. doi:10.1016/j.jcsr.2008.07.011.

Buchanan, D., Real, E., Gardner, L., 2018. Testing, simulation and design of cold-formed stainless steel CHS columns. Thin-Walled Structures vol. 130 p.297-312. ISSN: 0263-8231. doi:10.1016/j.tws.2018.05.006.

Buchanan, D., Zhao, O., Real, E., Gardner, L., 2020. Cold-formed stainless steel CHS beam-columns - Testing, simulation and design. Engineering Structures vol. 213. ISSN: 0141-0296. doi:10.1016/j.engstruct.2020.110270.

Daghash, S.M., Huang, Q.D., Ozbulut O.E., 2019. Tensile Behavior and Cost-Efficiency Evaluation of ASTM A1010 Steel for Bridge Construction. Journal of Bridge Engineering vol.24 iss.8. ISSN (online): 1943-5592. doi: 10.1061/(ASCE)BE.1943-5592.0001449.

Gardner, L., Nethercot, D.A., 2001. Numerical modelling of cold-formed stainless steel sections, In: Mäkeläinen, et al., editors. Proceedings of the 9th Nordic Steel Construction Conference, Helsinki, Finland. p.781-789.

Gardner, L., Nethercot, D.A., 2004. Experiments on stainless steel hollow sections - Part 1: Material and cross-sectional behaviour. Journal of Constructional Steel Research vol.60 p. 1291-1318. doi:10.1016/j.jcsr.2003.11.006.

Hill, H.N. 1994. Determination of stress-strain relations from the offset yield strength values. Technical Note No. 927. National Advisory Committee for Aeronautics, Washington D.C.

Jindra, D., Kala, Z., Seitl, S., Kala, J., 2020. Material model parameter identification of stainless steel (AISI 304L). Proceedings of 26th International Conference Engineering Mechanics 2020, Brno, Czech Republic, 24.-25.11.2020. ISSN: 1805-8248. ISBN: 978-80-214-5896-3.

Mirambell, E., Real, E., 2000 On the calculation of deflections in structural stainless steel beams: an experimental and numerical investigation. Journal of Constructional Research vol.54 p.109-133.

Ramberg, W., Osgood, W.R., 1943. Description of stress-strain curves by three parameters. Technical Note No. 902. National Advisory Committee for Aeronautics, Washington D.C.